Journal of Molecular Structure 1165 (2018) 332–343

Contents lists available at ScienceDirect

Journal of Molecular Structure

journal homepage: http://www.elsevier.com/locate/molstruc

Synthesis, spectroscopic characterization and structural study of 2-isopropenyl-3-methylphenol, carquejiphenol, a carquejol derivative with potential medicinal use

Manuel Minteguiaga [a, b], Eduardo Dellacassa [b], Maximiliano A. Iramain [c], Cesar A.N. Catalán [a], Silvia Antonia Brandán [c, *]

[a] INQUINOA-CONICET, Instituto de Química Orgánica, Facultad de Bioquímica, Química y Farmacia, Universidad Nacional de Tucumán, Ayacucho 471, T4000INI, San Miguel de Tucumán, Argentina
[b] Laboratorio de Biotecnología de Aromas, Departamento de Química Orgánica, Facultad de Química, Universidad de la República, General Flores 2124, Montevideo, 11800, Uruguay
[c] Cátedra de Química General, Instituto de Química Inorgánica, Facultad de Bioquímica, Química y Farmacia, Universidad Nacional de Tucumán, Ayacucho 471, 4000, San Miguel de Tucumán, Tucumán, Argentina

ARTICLE INFO

Article history:
Received 30 October 2017
Received in revised form
29 March 2018
Accepted 2 April 2018
Available online 3 April 2018

Keywords:
Carquejiphenol
Vibrational spectra
Molecular structure
Force field
DFT calculations

ABSTRACT

In this work, 2-isopropenyl-3-methylphenol, hereafter referred to as carquejiphenol (CARP), a minor component of "carqueja" essential oil, was synthesized starting from carquejol and characterized by using Fourier Transform infrared (FT-IR) and Raman (FT-Raman) spectroscopies, Ultraviolet–Visible (UV–Visible) spectroscopy, Electron Impact Mass spectrometry (EI-MS), Hydrogen and Carbon Nuclear Magnetic Resonance (^{1}H- and ^{13}C-NMR) and 2D ^{1}H–^{1}H gCOSY, ^{1}H–^{13}C gHSQC, ^{1}H–^{13}C gHMBC experiments. A very good correlation between the predicted FTIR, FTRaman, UV–visible and ^{1}H–^{13}C-NMR spectra for monomer and dimer of CARP by using theoretical B3LYP/6-31G* and 6-311++G** calculations with the corresponding experimental ones was observed. The solvation energies for CARP were predicted by using both levels of calculations and considering the solvent effects with the polarised continuum and solvation models. The increase in volume in solution supports the H bonds formation due to the presence in its structure of an OH group, as revealed by atoms in molecules (AIM) analysis. A high stability for CARP was found by using natural bond orbital (NBO) and AIM studies, while the investigation of the frontier orbitals reveals that CARP is more reactive than carquejol and N-(3,4-dimethoxybenzyl)-hexadecanamide but less reactive than the sesquiterpene lactone cnicin. The proximity of both the electrophilicy and nucleophilicity index of CARP with those obtained respectively for carquejol and for N-(3,4-dimethoxybenzyl)-hexadecanamide, suggests that CARP could probably present pharmacological properties. The scaled quantum mechanical force field (SQMFF) methodology was used to compute the harmonic force fields and to perform the complete vibrational analysis. In this way, 63 normal modes of vibration were assigned and compared with other terpene substances.

1. Introduction

In the present work we have synthesized 2-isopropenyl-3-methylphenol, one of the products formed by air oxidation of carquejol [1] that, by simplicity, we have called carquejiphenol (CARP). Carquejol, carquejyl acetate and eventually carquejiphenol are distinctive components of the essential oil of *Baccharis trimera* (Less.) DC (syn. *B. genistelloides* Pers. and *B. triptera* Mart.; vernacular name "carqueja") (Asteraceae), a medicinal and aromatic plant native to the Southern Cone of South America [1,2]. In particular, these derivatives are interesting from the pharmacological and medicinal point of view because they have curative properties [2–12] such as anti-inflammatory, analgesic, antifungal, antiviral, antimicrobial [2–6] and cytotoxic [7,10]. Recently, we have isolated carquejol from *Baccharis trimera* which was characterized by FT-IR, FT-Raman, UV–Visible, electronic circular dichroism (ECD), Mass, ^{1}H- and ^{13}C-NMR and 2D ^{1}H–^{1}H gCOSY, ^{1}H–^{13}C gHSQC, ^{1}H–^{13}C

* Corresponding author.
E-mail addresses: sbrandan@fbqf.unt.edu.ar, brandansa@yahoo.com.ar (S.A. Brandán).

https://doi.org/10.1016/j.molstruc.2018.04.001
0022-2860/

gHMBC spectroscopies [13]. Its structural, electronic, topological and vibrational properties were also studied combining the experimental data with density functional theory (DFT) calculations [14,15]. Because carquejol is a monoterpene alcohol with two chiral centres, its four possible stereostructures were considered but vibrational circular dichroism (VCD) studies [16] showed that the natural alcohol is constituted only by the (4S,5R) stereoisomer. The absolute configuration (4S,5R) was theoretically confirmed by the experimental ECD spectrum [13] whilst chiral analysis using a chiral selector capillary column CycloSil B (Agilent Technologies) confirmed that both carquejol and carquejyl acetate from *B. trimera* were enantiomerically pure [13]. The biological properties observed for carquejol could be attributed to the proximity of its nucleophilic index with those reported for other bioactive terpenes [17–22]. The predicted geometrical parameters, harmonic force fields and the complete vibrational assignments for the most stable conformations of carquejol were also reported [13]. On the other hand, molecular electrostatic potential (MEP) surfaces revealed that the nucleophilic and electrophilic sites of higher reactivity are principally centred on the OH group. At present, there is almost no data on CARP in the literature so it is interesting to study its structure and properties to compare them with those obtained for carquejol. At this point, we also expected that the presence of the CH_3, $H_2C{=}C{-}CH_3$ and OH groups on the benzene ring of CARP could give interesting results considering that, structurally, carquejol has similar groups. A remarkable difference between both compounds is that CARP do not present chiral C atoms and, for this reason, it is interesting to know all its conformers and properties. With this perspective, the purposes of this work are first, to synthesize CARP and later to characterize it by using FT-IR, FT-Raman, UV–Visible, EI-MS, ^{1}H- and ^{13}C-NMR and 2D ^{1}H–^{1}H gCOSY, ^{1}H–^{13}C gHSQC, ^{1}H–^{13}C gHMBC spectroscopies. At the same time, we aimed to combine these experimental data with those from theoretical DFT calculations using the hybrid B3LYP method together with the 6-31G* and 6-311++G** basis sets [23,24], and so to study the structural, electronic, topological and vibrational properties. Additionally, in order to identify CARP by using vibrational spectroscopy, it is very useful the determination of the harmonic force fields through the normal internal coordinates and the Scaled Quantum Mechanical Force Field (SQMFF) methodology [25] by using those two levels of theory. A dimeric species is also proposed for CARP, in agreement with other structures that contain a phenol group, because this group is considered a strong hydrogen-bond acceptor and donor [26]. Hence, experimental bands not justified by the monomeric species were attributed to that dimeric structure. A complete assignments of all bands observed in the vibrational spectra of CARP is presented. Finally, the frontier orbitals and a series of descriptors were also calculated in order to predict reactivity and behaviour by using both levels of theory [27–29]. These results were compared with those obtained for carquejol [13] and those calculated for other terpenic substances [27–29]. Some Lipisnki's and Veber's criteria were also applied for carquejiphenol in order to evaluate its pharmacological properties [30,31].

2. Experimental

Scheme for the synthesis of carquejiphenol (2-isopropenyl-3-methylphenol) from carquejol (see Scheme 1):

2.1. Obtention of carquejol

Carquejol was obtained from the essential oil of *Baccharis trimera* (Less.) DC as described in Ref. [13]. This oil was composed of 71.4% carquejyl acetate, 0.5% carquejol and 0.1% CARP according to the analysis by gas chromatography-mass spectrometry (GC-MS). Chiral analysis using the GC-MS equipment with a chiral selector capillary column CycloSil B, showed that both carquejol and carquejyl acetate from *B. trimera* were enantiomerically pure [13].

2.2. Oxidation of carquejol to carquejone with chromic acid in acetone

The oxidant reagent was prepared by dissolving 0.67 g of chromium trioxide (CrO_3) in 0.60 mL of concentrated sulfuric acid and then diluted up to 5.0 mL with distilled water.

The oxidant reagent (2.0 mL) was then added dropwise (5 min) to carquejol (0.601 mg; 4 mmol) dissolved in freshly distilled acetone (8.0 mL) at 0 °C under continuous magnetic stirring. The progress of the reaction was monitored by thin layer chromatography (TLC) [13]. If necessary, additional 0.10 mL increments of oxidant reagent were added till complete disappearance of carquejol spot on TLC. The oxidant excess was destroyed by adding a few drops of methanol and the organic layer was decanted, diluted with hexane (10 mL), washed with brine (2 × 2 mL), dried (anhydrous Na_2SO_4) and the solvent evaporated to give 0.481 g of a yellowish oil (81% yield). The oil analyzed by GC-MS was composed of carquejone (93.6%), CARP (6.2%) and carquejol (0.2%). The oxidation step should be performed as quickly as possible to shorten the time that carquejona was in acidic conditions which catalyzes its isomerization to CARP. UV (ethanol) λ_{max} (log *e*) 220 nm (4.00). EI-MS (70 eV); m/z (%) $[M]^+$ 148 (11), 133 (40), 120 (20), 105 (100), 92 (28), 91 (45), 79 (71), 77 (39), 68 (21), 65 (13), 53 (10), 51 (15), 41 (9), 40 (9). ^{1}H-NMR (200 MHz, $CDCl_3$) δ 6.97 ddd (1H; 10, 4.8, 3; H-5); δ 6.11 ddd br (1H; 10, 3, 1.7; H-4); δ 5.00 br s (1H; H-7a); δ 4.96 m (fine splitting) (2H; H-7b + H-9a); δ 4.73 m (fine splitting) (1H; H-9b); δ 3.64 br s (1H; H-2); δ 3.18 dquint (1H; 20.4, *ca.* 2.5; H-6a); δ 3.00 dddd (1H; 20.4, 4.8, 1.7, 0.8; H-6b); δ 1.76 br s (3H; fine splitting, 0.7 Hz; H-10) (see Fig. S11a); ^{13}C-NMR (50 MHz, $CDCl_3$) δ 199.0 (C-3), 148.0 (C-5), 141.6 (C-1), 141.1 (C-8), 129.0 (C-4), 113.9 (C-7), 112.8 (C-9), 63.3 (C-2), 32.3 (C-6), 21.5 (C-10) (see Fig. S11b).

Carquejone is unstable and readily isomerizes to 3-methyl-2-isopropenylphenol by both alkalis and acids.

2.3. Alkaline isomerization of carquejone to carquejiphenol (3-methyl-2-isopropenylphenol)

A 5% aqueous solution of sodium hydroxide (2 mL) was added dropwise to 297 mg (2.0 mmol) of carquejone with magnetic stirring at room temperature. After 10 min, the mixture was acidified with 5% HCl and extracted with methylene chloride (3 × 5 mL). The

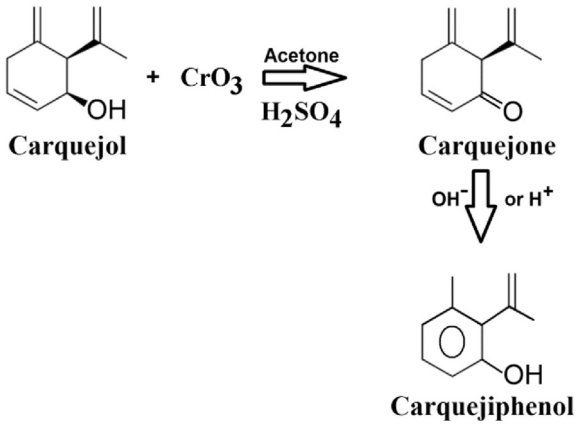

Scheme 1. Synthesis of carquejiphenol.

organic extracts were reunited, dried (anhydrous Na_2SO_4), filtered and evaporated to give 251 mg of an oily residue which was column chromatographed (Si gel 230–400 mesh) using a mixture of hexane-methylene chloride as eluting solvent yielding 155 mg (52% yield) of CARP. Needles, mp 41-43 °C (99.7% pure by GC-MS). UV (hexane) λ_{max} (log *e*) 210 nm (3.04), 279 nm (1.30). EI-MS (70 eV); m/z (%) $[M]^+$ 148 (75), 133 (61), 115 (19), 105 (100), 103 (17), 91 (20), 79 (14), 77 (27), 65 (7.5), 63 (9.5), 51 (10), 41 (2) (see Fig. 1). ^{1}H-NMR (200 MHz, $CDCl_3$) δ 7.07 dd (1H; 8 and 7.5 Hz; H-7), 6.78 br d (1H; 8 Hz; H-21), 6.76 br d (1H; 7.5 Hz; H-8), 5.52 dq (1H; 2 and 1.5 Hz; H-11), 5.38 br s (1H; disappears by exchange with D_2O; H-23), 5.06 dq (2 and 1 Hz; H-12), 2.25 br s (3H; H-18, H-19 and H-20); 2.03 dd (3H; 1.5 and 1 Hz; H-14, H-15 and H-16) (see Fig. S10a); ^{13}C-NMR (50 MHz, $CDCl_3$) δ 151.5 (C-6), 141.5 (C-9), 135.8 (C-4), 129.4 (C-5), 127.8 (C-2), 121.8 (C-3), 118.2 (C-10), 112.3 (C-1), 23.4 (C-13), 19.3 (C-17) (see Fig. S10b). IR and Raman spectra are shown in Figs. 5 and 6.

2.4. Acid isomerization of carquejone to carquejiphenol

To carquejone (31 mg) dissolved in benzene (0.8 mL), 85% formic acid (0.2 mL) was added and the mixture incubated 60 min at 70 °C with magnetic stirring. Then the reaction mixture was allowed to reach room temperature, diluted with dichloromethane (DCM) (20 mL), washed with 5% $NaHCO_3$ (3 × 5 mL), brine (2 × 3 mL) and dried (anhydrous Na_2SO_4). After filtering and solvent evaporation, the residue (20 mg, 64.5%) showed to be 98% CARP and 2% carquejone by GC-MS analysis.

2.5. General experimental procedures

The NMR experiments were conducted in a Bruker instrument at 200 MHz (^{1}H) and 50 MHz (^{13}C). All the spectra were recorded in chloroform-D1 (deuterium degree min. 99.8%, Sigma-Aldrich) with 0.03% TMS as internal reference. 2D NMR spectra (^{1}H–^{1}H gCOSY, ^{1}H–^{13}C gHSQC, ^{1}H–^{13}C gHMBC) were acquired using standard Bruker programs. All the GC-MS (EI-MS), UV, FT-Raman and FT-IR analysis were performed in the experimental conditions detailed previously [13].

3. Computational details

GaussView program [32] was used to model the initial CARP structure, while their optimizations were performed with the Gaussian 09 program [33] by using the hybrid B3LYP/6-31G* and B3LYP/6-311++G** methods [23,24]. For both structures, the potential energy surfaces (PES) described by the dihedral C6–C5–C9–C10 angles were studied with both levels of theory. Fig. S1 shows two stable conformers for CARP by using the B3LYP/6-31G* level of theory, named C1 and C2 where both structures have the same energies (−463.4930 a.u. in gas phase and −463.4997 a.u. in aqueous solution by using the B3LYP/6-31G* level of theory) and, as a consequence, the same properties are expected for both conformers in both media. The two most stable conformers of CARP are shown in Fig. 2. It is very interesting to study two charge's types in order to observe their differences, thus, the natural populations atomic (NPA) [34] charges and the Merz-Kollman (MK) [35] charges were used to calculate the molecular electrostatic potentials with the NBO program [34]. Bond orders and the donor-acceptor interactions were also calculated**.** The topological properties were also evaluated at the two levels of theory by using the AIM2000 program [36]. On the other hand, the normal internal coordinates built as other similar species with six member's rings [17–20,27–29] were employed together with the SQMFF methodology [25] and the Molvib program [37] in order to compute the force fields at the two levels of theory. To perform the complete vibrational assignments, a dimeric species of CARP was proposed as phenol groups are considered strong hydrogen-bond acceptors and donors according to Jelsch and Bisseyou [26]. Fig. 3 shows the theoretical structure proposed for the dimeric species. Here, the energy for the dimeric species is of −926.9976 a.u. by using the B3LYP/6-31G* level of theory and their value decreases when it is corrected by basis set superposition error (BSSE) [38]. Hence, experimental bands not justified by the monomeric species can be easily attributed to that dimeric structure. Furthermore, the complete assignments of all bands observed in the vibrational spectra of CARP were performed considering both IR and Raman spectra and using for the monomer the potential energy distribution (PED) contribution ≥ 10%. For the dimeric species, the *GaussView* program [32] was used as an aid to perform the vibrational assignments. On the other hand, the Gauge-Independent Atomic Orbital (GIAO) method [39] was employed to predict the ^{1}H and ^{13}C chemical shifts with both methods, using Tetramethylsilane (TMS) as reference. In the same way, the predicted ultraviolet–visible spectrum for CARP in water was computed by using Time-dependent DFT calculations (TD-DFT) with both levels of theory and the Gaussian 09 program [33]. Due to the presence of an

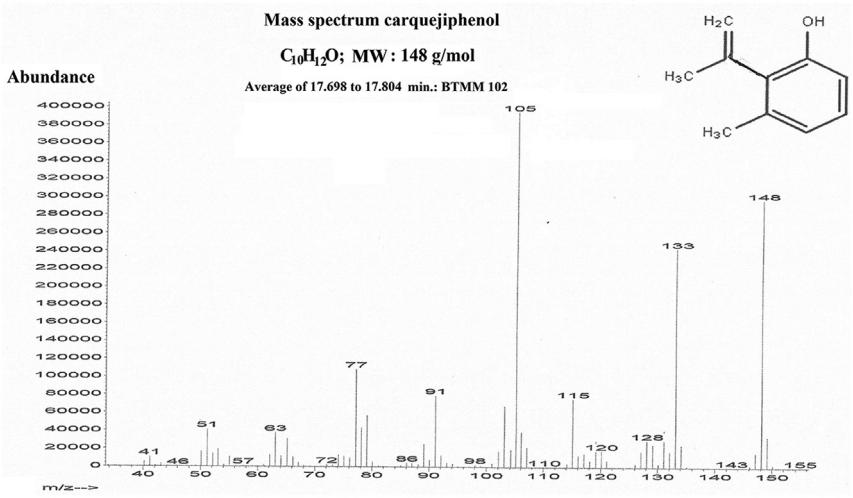

Fig. 1. Mass spectrum of carquejiphenol obtained by using Electron Impact Mass Spectrum and an ionization potential of 70 eV.

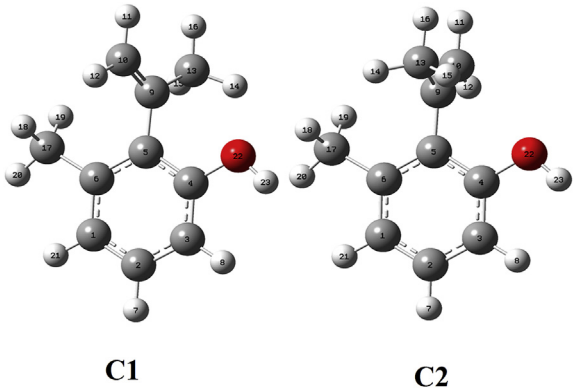

Fig. 2. Theoretical molecular structures of the most stable C1 and C2 conformers of carquejiphenol and atoms numbering (*GaussView* program).

isopropenyl group in the CARP structure in similar form than carquejol, it was necessary to predict their reactivity and behaviour. Hence, the frontier orbitals and the chemical potential (μ), electronegativity (χ), global hardness (η), global softness (S), global electrophilicity index (ω) and nucleophilicity indexes (E) descriptors were computed [13,17–21,27,29] by using both methods and data later compared with those from other terpenic substances [17–21]. In addition, the pharmacological properties of carquejiphenol were also evaluated by using some Lipisnki's and Veber's criteria [30,31].

4. Results and discussion

4.1. Structural study in gas phase and in aqueous solution

Total and relative energies, dipolar moments and volume variations for the most stable structure of CARP in gas and aqueous solution phases are summarized in Table 1 together with the solvation energy values by using both basis sets. The volume values were calculated with the Moldraw program [40], while the corrected solvation energies were computed taking into account the non-electrostatic terms with the polarised continuum and solvation PCM/SMD models [41–43] and the Gaussian program [33]. The uncorrected solvation energy values were calculated for both basis sets from the difference between the total energy values in solution and the values in gas phase. All energy values presented in Table 1 were corrected by the zero point vibrational energy (ZPVE) which is a correction to the electronic energy because the effects of molecular vibrations persist even at 0 K. Note that the uncorrected and corrected solvation energies slight increase their values by using the 6-31G* basis set but both decrease with the greater basis set. First, we observed that the dipole moment values with both basis sets increase in solution in accordance with their volumes and, that their variations also increase with the basis set. Thus, Fig. S2 shows the corresponding magnitudes and orientations of the dipole moment vectors for CARP in gas phase when increase the size of basis set at 6-311++G** basis set. Hence, higher total and solvation energies values were observed when increase the volume from 0.5 to 1.2 $Å^3$.

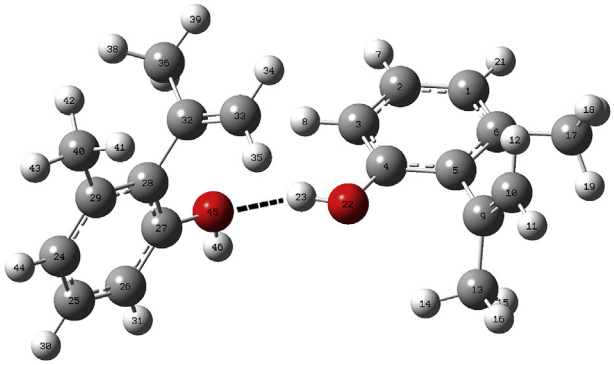

Fig. 3. Dimeric structure of the most stable C1 conformer of carquejiphenol and atoms numbering. The intra-molecular H bond is identified in dashed lines (*GaussView* program).

So far, the CARP structure was not experimentally determined, for this reason, the calculated geometrical parameters presented in Table 2 were compared with those theoretical corresponding to carquejol [13] and to diterpenic substances as cembrane diterpene [44] and 7-methyl-16-oxo-4,10-bis-(prop-1-en-2-yl)-17,18-dioxa-14,15-diaza-tetra-cyclo-[9.4.2.$1^{6,9}$.$0^{1,12}$]octa-deca-6,8,14-trien-5-yl acetate] (KAP) [45]. The structures of these compounds are given in Fig. S3. The root-mean-square deviation (RMSD) values were used to see the correlations in the bond lengths and angles between experimental and calculated values. Here, the better bond lengths correlations are observed for the isopropenyl group in relation to those corresponding to the ring (0.101–0.099 Å), as can be seen in Table 2. Fig. 4 shows clearly the differences between the bond lengths of carquejol with those corresponding to carquejiphenol. Hence, in CARP the ring is planar and as a consequence the distances from C1–C2 to C6–C1 are lower in CARP than carquejol with the exception of the C2–C3 distance that is surprisingly minor in carquejol than CARP because it is the only double bond observed in the carquejol ring. On the other hand, the C5–C9, C9=C10 and C9–C13 distances corresponding to the isopropenyl groups in carquejol and CARP are practically the same while the C4–O22 distance in CARP is lower, as expected because the C4 atom in carquejol has sp^3 hybridization while that atom in CARP has sp^2 hybridization. For the bond angles, we also observed the better correlations for the isopropenyl group while not very good correlations are observed when the dihedral angles of CARP are compared with the corresponding to carquejol. In particular, the dihedral C10 = C9–C5–C4 angle related to the isopropenyl group in CARP (−106.5°, by using 6-311++G** basis set) is very similar to that experimental value of −92.5° observed in the crystalline kallolide A acetate pyrazoline structure [45]. In the dimeric CARP structure are expected inter-molecular H bonds because of the presence of OH groups which are strong hydrogen-bond acceptors and donors [26], as are indicated in Fig. 3 by means of dashed lines. Here, the interaction energy for the dimeric species, calculated taking into account the BSSE energy by using 6-31G* basis set, is 10.23 kJ/mol which results from the difference between the uncorrected energy of −926.9976 and the corrected energy by BSSE of −926.9937 a.u.

4.2. NPA and MK charges, MEP and bond orders

The investigations on the hydrophobic and hydrophilic sites and the atomic charges involved in all bonds are of interest in CARP because this species could have potential pharmacological properties as was reported for carquejol [13]. Hence, for CARP by using both basis sets were studied the atomic natural population (NPA) and Merz-Kollman (MK) charges together with the molecular electrostatic potential (MEP) values [35]. The bond orders expressed as Wiberg indexes were also calculated in order to investigate the characteristics of all their bonds by using the two levels of theory. Thus, in Table S1 are summarized the calculated MK and NPA charges, the molecular electrostatic potential and the bond order values. The behaviours of both MK and NPA charges on

Table 1
Calculated total energies (*E*), relative (Δ*E*), dipole moments (μ), volume variations (ΔV) and solvation energies (ΔG) for carquejiphenol in gas and aqueous solution phases by using two level of theory.

B3LYP/6-31G*				
Property	Gas phase	PCM	ΔE(kJ/mol)	ΔV(Å^3)
E (Hartrees)	−463.4930	−463.4997	−15.57	
μ(D)	1.27	1.77		
V(Å^3)	178.4	178.9		0.5
B3LYP/6-311++G**				
Property	Gas phase	PCM	ΔE(kJ/mol)	ΔV(Å^3)
E (Hartrees)	−463.6263	−463.6340	−20.20	
μ(D)	1.13	1.69		
V(Å^3)	177.5	178.7		1.2
Solvation energy (kJ/mol)				
Basis set	$\Delta G_u^{\#}$	ΔG_{ne}	ΔG_c	
6-31G*	−15.57	21.57	−37.14	
6-311++G**	−20.20	22.78	−42.98	
Species	Gas phase	PCM	ΔE(kJ/mol)	
Corrections **Z.P.V.E**				
Basis set	E (Hartrees)		(kJ/mol)	
	Gas phase	PCM	$\Delta E = \Delta G_u^{\#}$	ΔG_c
6-31G*	−463.6866	−463.6932	−17.31	−38.88
6-311++G**	−463.8182	−463.8257	−19.67	−42.45

$\Delta G_u^{\#}$, See text, **Z.P.V.E,** zero point vibrational energy.

Table 2
Comparison of calculated geometrical parameters for carquejiphenol with the corresponding theoretical for carquejol and experimental ones for other terpenes.

Parameters	B3LYP method			Exp[c]	Exp[d]
	Carquejiphenol[a]		Carquejol[b]		
	6-31G*	6-311++G**	6-31G*		
Bond lengths (Å)					
C1–C2	1.392	1.390	1.510	1.508	
C2–C3	1.392	1.390	1.334	1.334	
C3–C4	1.396	1.394	1.514	1.490	
C4–C5	1.407	1.404	1.546	1.550	
C5–C6	1.409	1.408	1.526		
C6–C1	1.402	1.400	1.514		
C5–C9	1.499	1.498	1.531		1.524
C9=C10	1.337	1.333	1.335		1.385
C9–C13	1.511	1.509	1.512		1.524
C6–C17	1.513	1.511			
C4–O22	1.372	1.373	1.429	1.428	
RMSD[b]	**0.090**	**0.091**			
RMSD[c]	**0.099**	**0.101**			
RMSD[d]	**0.032**	**0.035**			
Bond angles (°)					
C3–C4–O22	121.5	121.4	112.4	107.8	
C5–C4–O22	117.0	117.1	109.2	112.6	
C4–C5–C9	119.3	119.3	117.3		
C6–C5–C9	122.0	121.9	110.4		
C10 = C9–C13	122.2	122.5	121.1		122.2
C10 = C9–C5	121.1	121.1	125.1		119.3
C13–C9–C5	116.5	116.3	113.6		118.3
C1–C6–C17	119.2	119.2			
C5–C6–C17	121.1	121.2			
RMSD[b]	**6.6**	**6.6**			
RMSD[b]	**10.2**	**10.1**			
RMSD[c]	**1.5**	**1.6**			
Dihedral angles (°)					
C10 = C9–C5–C6	72.7	74.7	107.0		
C10 = C9–C5–C4	−108.7	−106.5	−16.0		−92.5
C13–C9–C5–C4	71.5	73.4			
H23–O22–C4–C3	−179.5	179.6	65.5		
O22–C4–C3–C2			145.2	146.1	

[a] This work.
[b] From Ref [13].
[c] From Ref [37] for.
[d] From Ref [38].

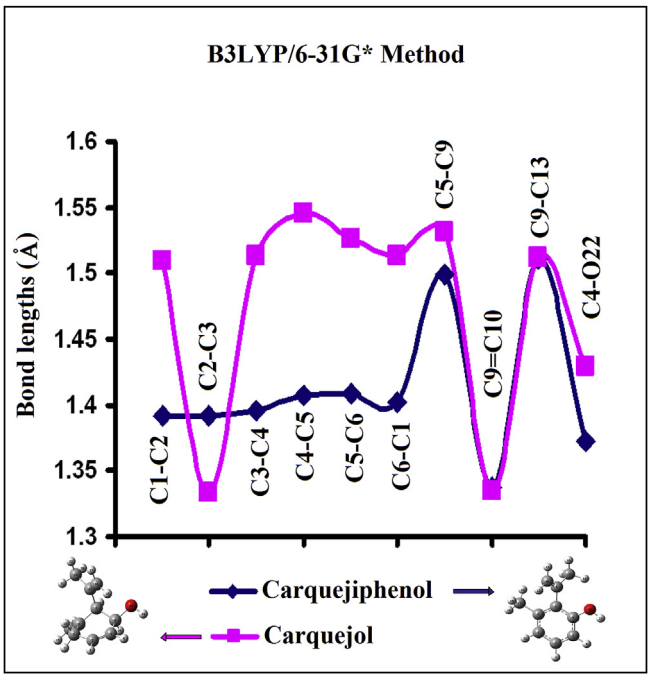

Fig. 4. Variations of the C-C and C-O bond lengths of carquejiphenol with those corresponding to carquejol in gas phase by using B3LYP/6-31G* level of theory. The structures of both species are also presented.

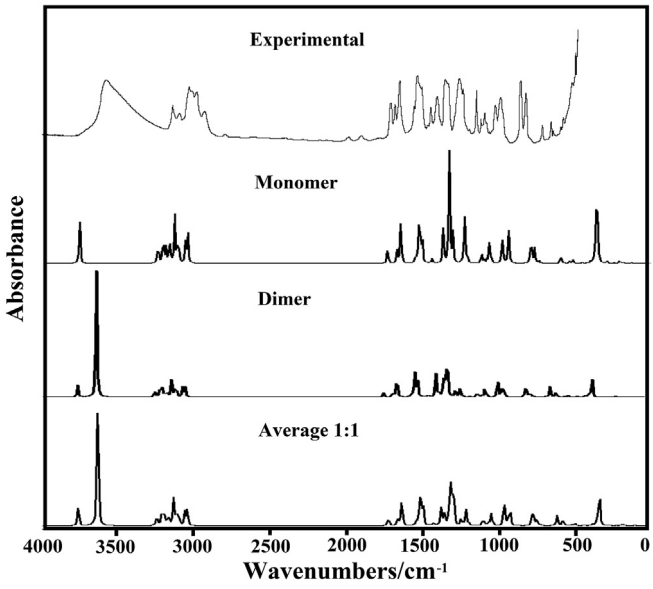

Fig. 5. Experimental infrared spectrum of carquejiphenol in the solid state compared with the corresponding predicted for C1 and with the predicted for the two monomeric and dimeric species by using B3LYP/6-31G* frequencies and intensities Lorentzian band shapes for a population 1:1 ratio for each species.

the C atoms by using both levels of theory are easily observed in Fig. S4. Both basis sets show practically the same behaviours of both MK and NPA charges on all C atoms but, in particular, the NPA charge on the C3 atom is slightly higher than the corresponding MK by using the 6-311++G** basis set while the MK charges on the C3 and C17 atoms are higher by using the 6-31G + basis set. On the other side, we observed that the MK charges on the C4, C6 and C9 are higher than the other ones.

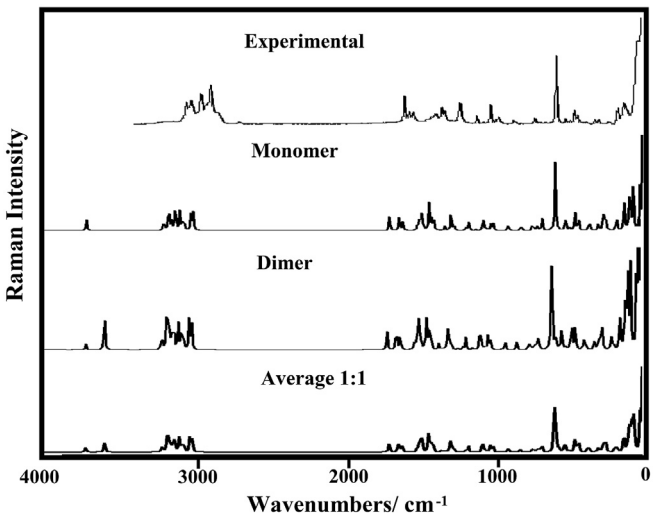

Fig. 6. Experimental Raman spectrum of carquejiphenol in the solid state compared with the corresponding predicted for C1 and with the predicted for the two monomeric and dimeric species by using B3LYP/6-31G* frequencies and intensities Lorentzian band shapes for a population 1:1 ratio for each species.

In relation to the molecular electrostatic potential (MEP) values, the values observed in Table S1 were calculated for all atoms from the atomic Merz-Kollman (MK) charges [35] with the Gaussian 09 program [33] while the MEP mapped surfaces were built with the *GaussView* program [32]. When the MEP values are represented in a graphic (see Fig. S5) in order to examine their variations, we observed practically the same behaviours with both basis sets and, the higher values are observed on the C4 atom, as expected because this is linked to the O atom of the OH group. Besides, the MEP values on all atoms are more negative by using the 6-311++G** basis set. When, the mapped MEP surface, presented in Fig. S6, was analyzed, we observed the same red and blue colorations on the OH group, as was also observed in carquejol. Hence, the nucleophilic and electrophilic sites, identified by the red and blue colours respectively, are located on the OH groups. Here, obviously the H23 atom linked to the O24 atom presents the less negative values with both basis sets because they are the most labile. Probably, this similarity in the MEP surface of CARP could be related to a potential pharmacological property, as compared with carquejol.

Table S1 shows the bond order (BO) expressed as Wiberg indexes for CARP by using both levels of theory. Analyzing the behaviours of all BO values of the C atoms, represented in Fig. S7, similar variations are observed with both basis sets but the C5, C6 and C9 atoms present the higher values. These atoms are respectively linked to the isopropenyl, methyl and $H_3C13–C9=C10$ groups, as observed in Fig. 2. Fig. S7 also shows that the 6-311++G** basis set predicted higher BO values for practically all atoms, in particular the C13 and C17 atoms.

4.3. Stability studies

NBO [34] and AIM [36] calculations were used to investigate the stability of CARP in gas phase by using the hybrid B3LYP method and the two 6-31G* and 6-311++G** levels of theory. In Table S2 are summarized the most important donor-acceptor energy interactions while in Table S3 are presented their topological properties. Regarding first the donor-acceptor energy interactions, we clearly observed that by using the higher size of the basis set enhance the number of contributions to the stability increasing significantly the total energy from 1352.85 to 6048.63 kJ/mol. Thus,

the new $\Delta ET_{\sigma \rightarrow \sigma^*}$ $\Delta ET_{LP \rightarrow \sigma^*}$ and $\Delta ET_{LP \rightarrow \pi^*}$ delocalizations only appear when the 6-311++G** basis set is used. Evidently, the donor-acceptor energy interactions are strongly dependent of the size of the basis set, as was also observed in carquejol [13]. Here, the $\Delta ET_{\pi \rightarrow \pi^*}$ interactions are observed with both basis sets.

The atoms in molecules theory (AIM) [46] is interesting to study the different interactions types expected in a molecule. The AIM2000 program [36] was employed to compute the topological properties, as recommended by Bader's theory [46]. Thus, the electron density distribution, $\rho(r)$ (BCPs) and the Laplacian values, $\nabla^2\rho(r)$ in the bond critical points were calculated together with the eigenvalues $(\lambda 1, \lambda 2, \lambda 3)$ of the Hessian matrix and the $\lambda 1/\lambda 3$ ratio. Table S3 shows those parameters calculated for both basis sets. Here, the properties computed in the bond critical points (BCPs) and ring critical points (RCPs) with both levels of theory show closed-shell interaction where $\lambda 1/\lambda 3 < 1$ and $\nabla^2\rho(r) > 0$. Thus, we observed the clear intra-molecular H bond formation with both basis sets, which is the O22—H14 interaction. The exhaustive inspection of the values showed that the properties are slightly higher by using the 6-31G* basis set. Here, the RCP belong to the ring while RCPN is the new RCP formed by the H bond interaction. The details of the molecular model for CARP in gas phase by using 6-31G* basis set can be seen in Fig. S8. Evidently, these two NBO and AIM studies support the high stability of CARP due to the donor-acceptor energies and to the intra-molecular interactions.

4.4. Frontier orbitals and descriptors

It is well known that the reactivities of different species can be predicted by using the frontier orbitals, as reported by Parr and Pearson [47]. Also, the behaviours of diverse systems can be predicted by means of the calculations of parameters identified as descriptors, which are broadly reported in the literature [17–20,29]. Here, Table S4 shows the calculated HOMO and LUMO orbitals, energy band gap, chemical potential, electronegativity (χ), global hardness (η), global softness (S), global electrophilicity index (ω) and global nucleophilicity index (E) for CARP by using the hybrid B3LYP level of theory and the 6-31G* and 6-311++G** basis sets. The equations used to calculate these parameters can also be seen in Table S4. The values were compared with those obtained for carquejol [13] and for terpene substances, as N-(3,4-dimethoxybenzyl)-hexadecanamide (DMH) [29] and cnicin [19] because for these two compounds it has been reported biological activities. Fig. S9 shows the behaviors of the Frontier orbitals and descriptors calculated for CARP in gas phase at the B3LYP/6-31G* level of theory and for the previously mentioned compounds. From the gap values with both basis sets, we observed that CARP is more reactive than carquejol and DMH, but cnicin is the most reactive of all them, as observed in Fig. S9. This fact is clearly justified because cnicin is a terpenic compound with various OH, C=O, C=C groups in their structure which confer to it interesting biological properties. Fig. S9 shows the behaviour of all the descriptors where clearly it is observed that cnicin has a high electrophilicity index. Note that the nucleophilicity index of carquejol is similar to that observed for cnicin while this index in CARP is similar to that observed for DMH. On the contrary, the electrophilicity index for CARP is similar to that observed for carquejol by using the same basis set and, as a consequence CARP could present similar properties than carquejol.

In this work, only three of the four Lipisnki's and Veber's criteria were applied for carquejiphenol in order to evaluate its pharmacological properties [30,31]. Hence, according to the rule of 5′ states, carquejiphenol could present absorption or permeation due to that: (i) CARP has one donor OH group (<number than 5 H-bond donors), (ii) the molecular weight (MWT) is <<< than 500 and, (iii) CARP has only an H-bond acceptor O atom (<10 H-bond acceptor). Consequently, pharmacological properties could be expected for carquejiphenol.

4.5. NMR study

Figs. S10a and S10b show the experimental ^{1}H and ^{13}C NMR spectra of CARP in $CDCl_3$, respectively while the 2D ^{1}H–^{1}H gCOSY, ^{1}H–^{13}C gHMBC and ^{1}H–^{13}C gHSQC spectra are given in Figs. S10c, S10d and S10f, respectively. Here, these 2D spectra were used for multiplicity determinations and were very important because they showed the spin-spin coupling between the hydrogen atoms of the molecule (gCOSY experiment), hydrogen atoms directly bonded to carbon (HSQC experiment) and long distance (two and three bonds) correlation of C with H (HMBC experiment). On the other hand, in Tables S5 and S6 are presented the predicted ^{1}H and ^{13}C NMR chemical shifts for carquejiphenol by using the GIAO method [39] calculated with both basis sets and compared with the corresponding experimental ones by means of the RMSD values. As observed in other compounds [13,17–20], the theoretical calculations overestimated the values in relation to the experimental ones, hence, a better correlation is observed for the ^{1}H nucleus (0.4–0.3 ppm) while for the ^{13}C nucleus (7.0–6.8 ppm) the values slightly increase. Here, we observed that the increase in the size of the basis set from 6 to 31G* to 6-311++G** improve notably the results especially for the ^{1}H nucleus than the C atoms. The H atom that belongs to the OH group was not considered in the RMSD value because this chemical shift depends heavily on sample concentration and temperature.

4.6. Vibrational study

The experimental IR and Raman spectra of CARP in solid phase can be seen in Figs. 5 and 6, respectively compared to the corresponding predicted for the monomer and dimer species by using B3LYP/6-31G* frequencies and intensities Lorentzian band shapes for a 1:1 population ratio of each species. Comparing first the IR spectra, a strong band at 1317 cm^{-1} is observed in the spectrum predicted for the CARP monomer but in the average spectrum considering the dimeric species the intensity of that band decreases notably, as was experimentally observed. Hence, it is evident that the dimeric species should be considered because this species also justify the wide IR band in the region 3500-3400 cm^{-1} attributed to the H bonds formation, as revealed by the AIM analysis. On the other hand, when the predicted Raman spectra for monomer and dimer are transformed from scattering activities to intensities, by known equations [48,49], better correlations are observed between the predicted and experimental Raman spectra, as observed in Fig. 6. Both B3LYP calculations optimize the CARP structures with C_1 symmetries. Therefore, for CARP, 63 normal modes of vibration are expected, all active, in both spectra. In order to perform the complete vibrational analysis and assignments of all bands observed in both IR and Raman spectra, the SQMFF procedure [25] and the Molvib program [37] were used. Here, the normal internal coordinates for CARP were not presented because they are similar to other reported [13,17–20]. The harmonic force fields were calculated for both levels of theory but, the B3LYP/6-31G* method was employed in the assignments due to that the scale factors used here are valid for that level of theory [25]. For the monomeric species we have considered the potential energy distribution (PED) contributions $\geq$ 10% while the assignments for the dimeric species were carried out with the aid of the *GaussView* program [32]. The observed and calculated wavenumbers together with the assignments for CARP using the B3LYP/6-31G* method are presented in

Table 3 while the PED contributions corresponding to the normal vibration modes of the monomer in gas and in aqueous solution phases can be seen in Tables S7 and S8, respectively. Brief discussions on the assignments for some groups corresponding to monomer and dimer are presented below.

4.6.1. Band assignments of monomer

4.6.1.1. OH mode. Generally, in compounds containing this group, the OH stretching modes are assigned in the 3752-3430 cm^{-1} region [13,18–20,29,50,51], hence, in CARP these modes are easily assigned to the very strong IR band at 3514 cm^{-1} because they are predicted at 3597 cm^{-1} in gas phase, at 3572 cm^{-1} in aqueous solution and, in the dimer at 3624 cm^{-1}. In this region, as observed in Fig. 4, the bands are broads probably due to the H bonds formation because the OH groups are strong hydrogen-bond acceptors and donors [27], as reported for thymidine by Görbitz et al. [50] and, as observed by the AIM study. The SQM calculations predicted the in-plane deformation or rocking modes for the CARP dimers at 1380 and 1358 cm^{-1} while for the monomer in gas phase at 1159 cm^{-1} and in solution at 1173 cm^{-1}.

4.6.1.2. CH modes. In CARP, the SQM/B3LYP/6-31G* calculations predicted the three expected C–H stretching modes between 3079 and 3044 cm^{-1}, this way, these modes for the monomer are clearly assigned to the IR band of medium intensity at 3077 cm^{-1}. In carquejol [13], the in-plane deformation or rocking modes are predicted between 1377 and 1157 cm^{-1}, hence, these modes in CARP are predicted between 1498 and 1106 cm^{-1} because all C–H groups are linked to C with sp^2 hybridization while in carquejol some C–H groups present sp^3 hybridization. Later, these modes are assigned to the IR and shoulder bands at 1483, 1464, 1455, 1256, 1185, 1160 and 1121 cm^{-1}. The out-of-phase modes in carquejol [13] are assigned in accordance with the calculations to the IR bands at 997, 985, 768, 726 and 700 cm^{-1}, in CARP; these modes are assigned to the IR and shoulder bands at 972, 900, 781 and 746 cm^{-1}

4.6.1.3. CH3 modes. CARP has two CH_3 groups and the expected six stretching modes are predicted as completely pure in the 3090-2914 cm^{-1} region. Thus, the antisymmetric and symmetric stretching modes are assigned to the IR bands at 3031, 2966, 2947 and 2919 cm^{-1}, as can be seen in Table 3. Obviously, the Raman bands observed with medium and strong intensities are evidently assigned to symmetrical modes. In carquejol [13], the CH_3 deformation modes are assigned between 1587 and 1436 cm^{-1} while the rocking and twisting modes are predicted between 1084/1026 and 220/171 cm^{-1}, here, these modes are predicted respectively in the 1461/1361, 1074/1010 and 210/108 cm^{-1} regions. Therefore, the IR and Raman bands observed in these regions were assigned to those vibration modes, as shown in Table 3.

4.6.1.4. CH_2 modes. Carquejol has two CH_2 groups with sp^2 hybridization and one CH_2 group with sp^3 hybridization while in CARP only a = CH_2 group is observed [13]. Thus, in carquejol the symmetrical = CH_2 groups modes are assigned to the very strong Raman band at 3032 cm^{-1}. Here, the antisymmetrical modes are predicted at 3102/3100 cm^{-1} whiles the corresponding symmetrical modes at 3026/3024 cm^{-1}. Thus, the CH_2 deformation, rocking, waging and twisting modes are predicted respectively in the 1400/1388, 1010/914, 919/918 and 671/666 cm^{-1} regions. Hence, they are assigned as can be seen in Table 3.

4.6.1.5. Skeletal modes. In carquejol [13], the C–O stretching modes are predicted between 1063 and 1020 cm^{-1} and assigned to 1065 cm^{-1}. Here, the very strong IR band at 1278 cm^{-1} is easily assigned to that mode corresponding to the monomer. In compounds containing C=C bonds, the corresponding stretching modes are assigned in the 1680-1659 cm^{-1} region [16–18]; therefore, in CARP those modes are assigned to the IR and Raman bands at 1638 and 1643 cm^{-1}. Note that the other expected C–C stretching modes corresponding to the ring are assigned to the bands in the 1610-1483 cm^{-1} region, as predicted by the SQM calculations. On the other side, the strong IR bands at 1074 and 914 cm^{-1} and the IR band of medium intensity at 947 cm^{-1} are associated to C–C stretching modes, as detailed in Table 3.

4.6.2. Band assignments of dimer

4.6.2.1. OH modes. Here, possibly the H bond formation in solution due to dimeric species shifts the OH stretching modes toward higher wavenumbers. Hence, the very strong IR bands at 3514 cm^{-1} is clearly assigned to those vibration modes. The in-plane deformation modes are predicted at 1380 and 1358 cm^{-1} and, for this reason, they are assigned to the Raman band and shoulder at 1395 and 1361 cm^{-1}, as indicted in Table 3. The out-of-plane deformation modes are predicted in the CARP dimer at 622 and 346 cm^{-1}. Hence, the IR band at 638 and 406 cm^{-1} and the Raman band at 332 cm^{-1} are assigned to those vibration modes, as observed in Table 3.

4.6.2.2. CH modes. In the dimer of CARP, the C–H stretching modes are predicted between 3163 and 3079 cm^{-1}, then, these modes are clearly assigned to the IR band of medium intensity at 3077 cm^{-1}. The in-plane deformation or rocking modes in the dimer are predicted between 1498 and 1106 cm^{-1}. Later, these modes are assigned to the IR and Raman bands observed in that region. According to the calculations, the out-of-phase modes are assigned to the IR bands at 951 and 558 cm-1.

4.6.2.3. CH_3 modes. In the dimeric species, the two stretching modes are predicted as practically pure in the 3090-3037 cm^{-1} region. Thus, both antisymmetric and symmetric stretching modes are assigned in that region, as can be seen in Table 3. In the dimer, the CH_3 deformation modes are predicted between 1447 and 1449 cm^{-1} while the rocking and twisting modes are predicted between 1074/1039 and 210/97 cm^{-1}, hence, they are assigned as predicted by calculations.

4.6.2.4. CH_2 modes. In the dimer the symmetric modes are predicted at 3053 cm^{-1} and, for these reasons, these modes are assigned to the Raman band of medium intensity at 3044 cm^{-1} while the CH_2 deformation, rocking, waging and twisting modes are predicted at higher wavenumbers than the corresponding to the monomer. Thus, for the dimer, these modes are predicted, respectively, in the 1464, 1074/1039, 943/927 and 764/730 cm^{-1} regions. Hence, they are assigned accordingly.

4.6.2.5. Skeletal modes. The IR band of medium intensity at 1333 cm^{-1} is associated to C–O stretching modes of the dimer while in this species, the C=C bonds are predicted in the 1726-1636 cm^{-1} region [17–20]; therefore, those modes are assigned to the Raman bands at 1643 and 1584 cm^{-1}. The C–C stretching modes are predicted between 1498 and 1295 cm^{-1}, as predicted by the calculations. The deformation and torsion ring modes are predicted for both monomer and dimer between 1119/499 and 737/97 cm^{-1}, as in similar compounds [17–20,29,50,51] and, as a consequence they were assigned in those regions.

5. Force field

The calculations of the frontier orbitals have evidenced that

Table 3
Observed and calculated wavenumbers (cm^{-1}) and assignments for carquejiphenol in gas phase and in aqueous solution and their dimer.

Experimental		B3LYP/6-31G* Method[a]					
		Monomer				Dimer	
		GAS		PCM		GAS	
IR	Raman	SQM[b]	Assignments	SQM[b]	Assignments	Calc[c]	Assignments
3514vs	3218vw	3597	νO22-H23	3572	νO22-H23	3624	νO-H
	3163vw	3102	ν_aCH_2	3100	ν_aCH_2	3200	νC-H
3077 m	3079 m	3071	νC2-H7	3078	νC2-H7	3188	νC-H
	3063w	3053	νC1-H21	3062	νC1-H21	3090	ν_aCH_3
	3044 m	3032	νC3-H8	3056	νC3-H8	3053	ν_sCH_2
3031w	3032sh	3026	ν_sCH_2	3024	ν_sCH_2	3037	ν_sCH_3
	3008w	2999	ν_aCH_3(C17)	3003	ν_aCH_3(C17)		
	2992sh	2998	ν_aCH_3(C13)	2998	ν_aCH_3(C13)		
	2981 m	2981	ν_aCH_3(C17)	2977	ν_aCH_3(C17)		
2966s	2977sh	2971	ν_aCH_3(C13)	2967	ν_aCH_3(C13)		
2947s	2947w	2928	ν_sCH_3(C17)	2926	ν_sCH_3(C17)		
2919s	2918s	2914	ν_sCH_3(C13)	2916	ν_sCH_3(C13)		
2865w	2871w						
1638 m	1643s	1659	νC9 = C10	1653	νC9 = C10	1726	νC = C
1610 m	1613 m	1606	νC3-C4νC1-C2νC4-C5	1603	νC3-C4νC4-C5	1641	νC-C
1580s	1584 m	1585	βC1-H21νC2-C3	1576	νC2-C3	1636	νC-C
1483 m	1493w	1487	νC5-C6	1481	βC1-H21νC5-C6	1498	βC-HνC-C
1464vs	1464w	1465	βC2-H7βC1-H21			1464	δCH_2
1455sh		1461	δ_aCH_3(C13)	1457	βC2-H7νC3-C4		
1455sh		1449	δ_aCH_3(C17)				
	1446sh	1445	δ_aCH_3(C17)			1447	δ_sCH_3
1433s		1440	δ_aCH_3(C13)	1436	δ_aCH_3(C13)		
1433s	1435w			1434	δ_aCH_3(C17)	1436	δ_sCH_3
1433s				1432	δ_aCH_3(C17)		
	1422sh			1426	δ_aCH_3(C13)	1429	δ_sCH_3
1394w	1395 m	1400	δCH_2	1388	δCH_2	1380	δO-H
1372 m	1378 m	1382	δ_sCH_3(C17)	1370	δ_sCH_3(C17)		
	1361sh	1368	δ_sCH_3(C13)	1361	δ_sCH_3(C13)	1358	δO-H
1333 m	1330vw					1330	νC-O
	1306sh			1305	νC5-C6νC1-C6	1304	νC-O
1290sh	1287sh	1305	νC5-C6			1295	νC-C
1278vs	1275s	1282	νC4-O22	1272	νC5-C9		
1278vs	1275s	1272	νC5-C9νC4-O22	1257	βC1-H21		
1278vs	1258sh	1255	βC1-H21	1251	νC4-O22	1251	βC-H
1185vs	1188vw	1167	βC2-H7	1173	δO-H	1199	βC-H
1160s	1165w	1159	δO-H	1153	βC2-H7βC3-H8	1154	βC-H
1121w	1121w	1122	βC3-H8	1119	βR_1	1106	βC-H
1074s	1076s	1077	βR_1νC1-C2	1074	νC1-C2	1074	ρCH_3 ρCH_2
		1057	$\rho'CH_3$(C13)	1052	$\rho'CH_3$(C13)	1053	ρCH_3
1043w	1044w	1047	$\rho'CH_3$(C17)	1044	$\rho'CH_3$(C17)	1040	ρCH_3
1043w	1044w					1039	ρCH_3 ρCH_2
1019w	1022w	1022	ρCH_3(C17)	1020	ρCH_3(C17)		
1005w	1004w	1012	ρCH_3(C13)	1010	ρCH_3(C13) ρCH_2		
988w	979vw					975	βR_1
972w	952vw	943	γC2-H7	958	γC2-H7	951	γC-H
947 m		940	νC6-C17	931	νC6-C17	943	$wagCH_2$
925sh	925w	918	$wagCH_2$	919	$wagCH_2$	927	$wagCH_2$
914s	910w	911	νC9-C13 ρCH_2	910	νC9-C13		
900sh	874w	850	γC3-H8γC1-H21	869	γC3-H8γC1-H21	868	γC-H
781vs	782w					785	γC-H
781vs	782w	777	βR_1	776	γC3-H8	780	γC-H
	761vw	768	γC4-O22	773	$\beta R_2\beta R_1$	764	τwCH_2
746s	746vw					752	γC-H
728sh	712vw	737	τR_1	737	τR_1	730	τwCH_2
	645vs					651	βR_1
	645vs	666	τwCH_2	671	τwCH_2	647	βR_1
638w	631sh	625	νC5-C9	626	νC5-C9νC6-C17	622	τOH
582w	582w					590	βR_3
582w	582w	574	$\beta C5-C9\beta R_3$	577	$\beta C5-C9\tau wCH_2$	579	τR_3
565w	568w	569	$\tau R_1\gamma C6-C17$	568	γC6-C17γC4-O22	558	γC-H
	550w	549	$\tau R_3\tau R_2$	552	$\tau R_3\tau R_2$	530	τR_2
518w	522w	521	βR_3	521	βR_3	528	βR_3
499w	502w	500	βR_2	499	βR_2	507	δCCC
471sh	483vw					506	δCCC
443w	468vw	440	βC4-O22γC9-C10	447	βC4-O22γC9-C10	456	γC-C
436w	446vw					442	γC-C
406w	392sh					394	τOH
399sh	388w	383	γC6-C17	385	$\tau R_3\gamma C6-C17$	389	τR_3
	345vw	357	βC6-C17 δC10C9C13	358	βC6-C17	358	δCCC
	332vw			337	τOH	346	τOH

Table 3 (*continued*)

Experimental		B3LYP/6-31G* Method[a]					
		Monomer				Dimer	
		GAS		PCM		GAS	
IR	Raman	SQM[b]	Assignments	SQM[b]	Assignments	Calc[c]	Assignments
	313vw	313	τOH			290	δCCC
	295w	278	δC10C9C13βC6-C17	275	δC10C9C13	277	δCCC
	237 m	227	τR_2	230	τR_2	210	τwCH_3
	196s	194	γC5-C9	198	τwCH_3(C13)	194	γC-C
	182sh	187	τwCH_3(C13)	189	γC5-C9	183	βC-C
	153sh	169	βC5-C9	168	βC5-C9	166	γC-C
	107s	108	τwCH_3(C17)	153	τwCH_3(C17)	120	τwCH_3
	93sh	94	τR_3βC9-C10	97	τR_3βC9-C10	97	τwCH_3
	67sh					73	γC-C
		49	τwCCC	52	τwCCC	49	δOH—O

Abbreviations ν, stretching; β, deformation in the plane; γ, deformation out of plane; wag, wagging; τ, torsion; β_R, deformation ring τ_R, torsion ring; ρ, rocking; τw, twisting; δ, deformation; a, antisymmetric; s, symmetric.
[a] This work.
[b] From scaled quantum mechanics force field.
[c] From B3LYP/6-31G* calculation.

CARP is more reactive than carquejol [13] and DMH [28] but, cnicin is the most reactive of all them. For these observations, it is very important to predict force constants in order to analyze the harmonic force of the different bonds in CARP. Thus, their force constants were calculated from the force fields in gas phase at the 6-31G* and 6-311++G** levels of theory and, later, they were compared in Table 4 with those reported for carquejol and other terpenic compounds, such as cnicin [19], 13-*epi*-sclareol [20] and onopordopicrin [18]. As it was explained in the section of computational details, the SQMFF approach [25] and the Molvib program [37] were used to obtain the scaled force fields at both levels of theory. First, we compared the force constants for CARP by using both levels of theory. Here, we observed a slightly increase in the *f(νO-H)* force constant when the size of the basis set increase from 6 to 31G* at 6-311++G** basis set but, a diminishing in the values for the *f(νC-H)*, *f(ν=CH₂)* and *f(νC-C)* force constants are observed while there are not observed changes in the values of the *f(δ=CH₂)* and *f(δC-OH)* force constants. When the values are compared with those calculated for carquejol by using 6-31G* basis set, the *f(νO-H)* force constant do not change but the *f(νC-H)* and *f(νC-C)* force constants decrease their values. The planarity of the ring in CARP justifies the difference in the *f(νC-C)* force constants while the existence in carquejol of a C—H bond where the C atom present a sp^3 hybridization probably could explain the diminishing in the *f(νC-H)* force constants because in CARP all C atoms of the ring have sp^2 hybridization.

6. Ultraviolet–visible spectrum

The UV—visible spectrum for CARP in aqueous solution was predicted by using TD-DFT calculations with the B3LYP/6-31G* method and the Gaussian program [33] while the experimental one was recorded in n-hexane solution. Both spectra are compared in Fig. 7. In the experimental spectrum two bands were observed, one intense at 210 nm and other of lower intensity at 279 nm together with a shoulder at approximately 190 nm, while the theoretical calculations predicted for CARP in aqueous solution a shoulder at 164 nm and two bands, one intense at 184.4 nm and other of lower intensity at 248 nm. There was very good concordance between the spectra but, evidently, the predicted spectrum is shifted toward lower wavelengths in relation to the experimental one. In phenol, two bands of approximately the same intensities at 200 and 269 nm are also observed as reported in Ref. [52]. These bands can be easily assigned to the $\pi \rightarrow \pi^*$ transitions due to the C=C double bonds, as predicted the NBO analysis and in agreement with literature data [53,54].

7. Conclusions

Carquejiphenol, a minor component of the *Baccharis trimera* essential oil, was synthesized and later characterized by using FT-IR, FT-Raman, UV—Visible, EI-MS, ^{1}H- and ^{13}C-NMR and 2D ^{1}H—^{1}H gCOSY, ^{1}H—^{13}C gHSQC, ^{1}H—^{13}C gHMBC spectroscopies. The molecular structure of the monomer and dimer were theoretically determined in gas phase by using the hybrid B3LYP method and the 6-31G* and 6-311++G** basis sets. Two structures with the same energies were found in the potential energy surface. The predicted FTIR, Raman, ^{1}H-NMR, ^{13}C-NMR and UV—visible spectra of both forms showed a very good correlation with the corresponding experimental ones. The predicted corrected solvation energies for CARP were also computed by using both levels of calculations and considering the solvent effects with the polarised continuum and solvation models. The increase in the volume in solution support the H bonds formation due to the presence of a OH group, as suggested in the literature and as revealed by AIM analysis. High

Table 4
Comparison of main scaled internal force constants for carquejiphenol in gas and aqueous solution phases compared with those calculated for carquejol.

B3LYP Method						
Force constant	Carquejiphenol[a]		6-31G*			
	6-31G*	6-311++G**	Carquejol[b]	Cnicin[c]	Epi[d]	Onopor[e]
f(νO-H)	7.20	7.40	7.20	6.99	6.92	7.16
f(νC-H)	5.10	5.07	4.80			4.96
f(ν=CH₂)	5.16	5.05	5.19	5.22	5.20	
f(νCH₂)			4.67	4.79	4.74	4.90
$f(\nu C\text{-}O)_c$			4.80	5.44	4.47	4.80
f(νC-C)	6.47	6.27	4.87			
f(δ=CH₂)	0.40	0.40	0.40	0.44	0.43	0.45
f(δCH₂)			0.80	0.76	0.76	0.77
f(δC-OH)	0.70	0.70	0.70			0.74

Units are mdyn Å^{-1} for stretching and mdyn Å rad^{-2} for angle deformations.
[a] This work.
[b] From Ref [13].
[c] From Ref [19] for.
[d] From Ref [20].
[e] From Ref [18].

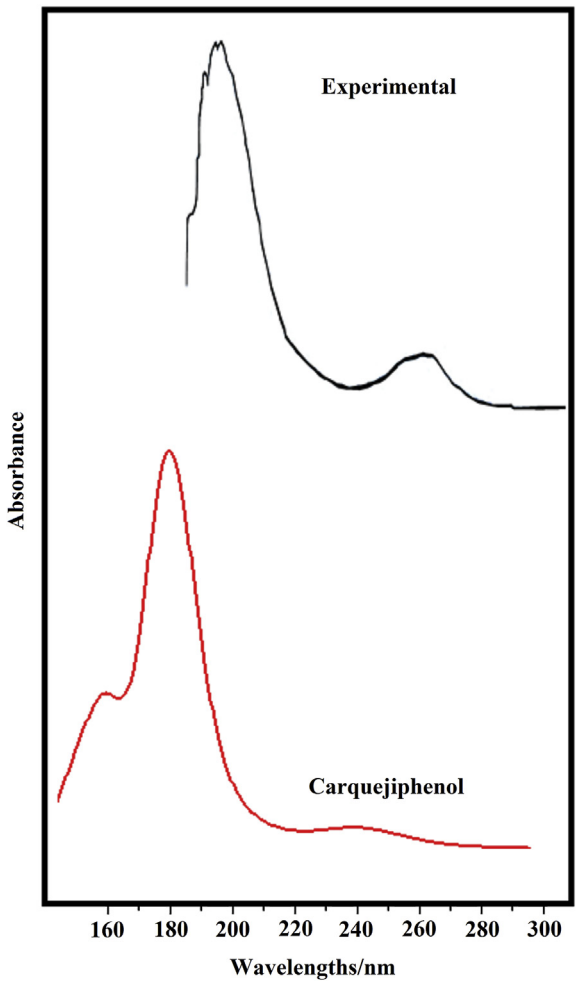

Fig. 7. Experimental UV–visible spectrum of carquejiphenol in n-hexane compared with the corresponding predicted for the monomeric and dimeric species by using B3LYP/6-31G* frequencies and intensities Lorentzian band shapes for a population 1:1 ratio for each species.

stability for CARP was found by using NBO and AIM studies, while the investigation of the frontier orbitals reveal that CARP is more reactive than carquejol and hexadecanamide but, the terpene cnicin is the most reactive. The proximities in the electrophilicy index of CARP with that obtained for carquejol and of the nucleophilicity index with that calculated for N-(3,4-dimethoxybenzyl)-hexadecanamide suggest probably that carquejiphenol could present pharmacological properties. The SQMFF methodology was used together with the Molvib program to compute the force fields and to perform the complete vibrational analysis. Hence, the 63 vibration normal modes were assigned and the force constants are also reported and compared with other reported from the literature.

Acknowledgements

This work was supported with grants from CIUNT Project 26/D207 and 26/D510 (Consejo de Investigaciones, Universidad Nacional de Tucumán) and CONICET (Consejo Nacional de Investigaciones Científicas y Técnicas, R. Argentina). MM thanks to ANII (Agencia Nacional de Investigación e Innovación, Uruguay) for PhD scholarships (POS-2011-1-3332 and POS NAC 2013-1-11316) and to Universidad Nacional de Tucumán (PEEP Program). The authors would like to thank Prof. Tom Sundius for his permission to use MOLVIB.

Appendix A. Supplementary data

Supplementary data related to this article can be found at https://doi.org/10.1016/j.molstruc.2018.04.001.

References

[1] Y.R. Naves, F. Caujolle, U.S. Patent 3,112 (1963) 245.
[2] C.A. Caneschi, F.J. Martins, D.G. Larrudé, E.C. Romani, M.A.F. Brandão, N.R.B. Raposo, *In vitro* antifungal activity of *Baccharis trimera* Less (DC) essential oil against dermatophytes, Trop. J. Pharmaceut. Res. 14 (2015) 2083–2089.
[3] F. Caujolle, D. Meynier, J. Cros, Pharmacological study of carquejol and its derivatives, Therapie 15 (1960) 931–939.
[4] R.M. Gené, C. Cartañá, T. Adzet, E. Marin, T. Parella, S. Cañigueral, Anti-inflammatory and analgesic activity of *Baccharis trimera*: identification of its active constituents, Planta Med. 62 (1996) 232–235.
[5] M.J. Abad, P. Bermejo, S. Sanchez Palomino, X. Chiriboga, L. Carrasco, Antiviral activity of some South American medicinal plants, Phytother Res. 13 (1999) 142–146.
[6] E.Y. Suzuki, C.A. Caneschi, R.C. Fochat, M.A.F. Brandão, N.R.B. Raposo, Antimicrobial activity of essential oil from *Baccharis trimera* (Less.) DC. (carqueja-amarga), Rev. Cubana Plant. Med. 21 (2016) 346–358.
[7] F.A. de Oliveira Garcia, M.M. Tanae, L.M. Brandão Torres, A.J. Lapa, M.T.R. de Lima-Landman, C. Souccar, A comparative study of two clerodane diterpenes from *Baccharis trimera* (Less.) DC. on the influx and mobilization of intracellular calcium in rat cardiomyocytes, Phytomedicine 21 (2014) 1021–1025.
[8] M.T. Gamberini, L.A. Skorupa, C. Souccar, A.J. Lapa, Inhibition of gastric secretion by a water extract from *Baccharis triptera* Mart, Mem. Inst. Oswaldo Cruz 86 (1991) 137–139.
[9] L.M.B. Torres, M.T. Gamberini, N.F. Roque, M.T.L. Landman, C. Souccar, A.J. Lapa, Diterpene from *Baccharistrimera* with a relaxant effect on rat vascular smooth muscle, Phytochemistry 55 (2000) 617–619.
[10] F. Fullas, R.A. Hussain, H.B. Chai, J.M. Pezzuto, D.D. Soejarto, A.D. Kinghorn, Cytotoxic constituents of Baccharis gaudichaudiana, J. Nat. Prod. 57 (1994) 801–807.
[11] L. Hennig, G.M. Garcia, A. Giannis, R.W. Bussmann, New constituents of *Baccharis genistelloides* (Lam.) Pers, ARKIVOC 6 (2011) 74–81.
[12] S. dos, S. Grecco, J.Q. Reimão, A.G. Tempone, P. Sartorelli, R.L.O.R. Cunha, P. Romoff, M.J.P. Ferreira, O.A. Fávero, João Henrique, G. Lago, In vitro antileishmanial and antitrypanosomal activities of flavanones from *Baccharis retusa* DC. (Asteraceae), Exp. Parasitol. 130 (2012) 141–145.
[13] M. Minteguiaga, E. Dellacassa, M.A. Iramain, C.A.N. Catalan, S.A. Brandan, A structural and spectroscopic study on carquejol, a relevant constituent of the medicinal plant *Baccharis trimera* (Less.) DC. (Asteraceae), J. Mol. Struct. 1150 (2017) 8–20.
[14] N.D. Yilmazer, M. Korth, Prospects of applying enhanced semi-empirical QM methods for 2101 virtual drug design, Curr. Med. Chem. 23 (20) (2016), 2101–2011.
[15] S. Superchi, P. Scafato, M. Gorecki, G. Pescitelli, Absolute configuration determination by quantum mechanical calculation of chiroptical spectra: basics and applications to fungal metabolites, Curr. Med. Chem. 25 (2) (2018) 287–320.
[16] G. Snatzke, A.F. Thomas, G. Ohloff, Die absolute konfiguration von carquejol und verwandten o-menthan-derivaten, Helv. Chim. Acta 52 (1969) 134–135.
[17] F. Chain, M.F. Ladetto, A. Grau, C.A.N. Catalán, S.A. Brandán, Structural, electronic, topological and vibrational properties of a series of N-benzylamides derived from Maca (*Lepidium meyenii*) combining spectroscopic studies with ONION calculations, J. Mol. Struct. 1105 (2016) 403–414.
[18] F. Chain, E. Romano, P. Leyton, C. Paipa, C.A.N. Catalán, M.A. Fortuna, S.A. Brandán, Vibrational and structural study of onopordopicrin based on the FTIR spectrum and DFT calculations, Spectrochim. Acta 150 (2015) 381–389.
[19] F. Chain, E. Romano, P. Leyton, C. Paipa, C.A.N. Catalán, M.A. Fortuna, S.A. Brandán, An experimental study of the structural and vibrational properties of sesquiterpene lactone cnicin using FT-IR, FT-Raman, UV–visible and NMR spectroscopies, J. Mol. Struct. 1065–1066 (2014) 160–169.
[20] F.E. Chain, P. Leyton, C. Paipa, M. Fortuna, S.A. Brandán, F.T.-I.R. FT-Raman, UV-Visible, and NMR spectroscopy and vibrational properties of the labdane-type diterpene 13-epi-sclareol, Spectrochim. Acta, Part A 138 (2015) 303–313.
[21] J. Pokorny, L. Borkova, M. Urban, Click reactions in chemistry of triterpenes-advances towards development of potential therapeutics, Curr. Med. Chem. 25 (5) (2018) 636–658.
[22] C. Zhong, N.R. Wall, Y. Zu, G. Sui, Therapeutic application of natural medicine monomers in cancer treatment, Curr. Med. Chem. 24 (34) (2017) 3681–3697.
[23] A.D. Becke, Density-functional exchange-energy approximation with correct asymptotic behavior, Phys. Rev. A38 (1988) 3098–3100.
[24] C. Lee, W. Yang, R.G. Parr, Development of the Colle-Salvetti correlation-energy formula into a functional of the electron density, Phys. Rev. B 37 (1988) 785–789.
[25] a) G. Rauhut, P. Pulay, Transferable scaling factors for density functional

derived vibrational force fields, J. Phys. Chem. 99 (1995) 3093–3099;
b) G. Rauhut, P. Pulay, Erratum to: transferable scaling factors for density functional derived vibrational force fields, J. Phys. Chem. 99 (1995) 14572.
[26] C. Jelsch, Y.B.M. Bisseyou, Atom interaction propensities of oxygenated chemical functions in crystal packings, IUCrJ 4 (2017) 158–174.
[27] E. Romano, L. Davies, S.A. Brandán, Structural properties and FTIR-Raman spectra of the anti-hypertensive clonidine hydrochloride agent and their dimeric species, J. Mol. Struct. 1133 (2017) 226–235.
[28] A. Hedoux, Y. Guinet, L. Carpentier, L. Paccou, P. Derollez, S.A. Brandán, Structural and vibrational characterization of sugar arabinitol structures employing micro-Raman spectra and DFT calculations, J. Mol. Struct. 1138 (2017) 118–128.
[29] F. Chain, M.A. Iramain, A. Grau, C.A.N. Catalán, S.A. Brandán, Evaluation of the structural, electronic, topological and vibrational properties of N-(3,4-dimethoxybenzyl)-hexadecanamide isolated from Maca (*Lepidium meyenii*) using different spectroscopic techniques, J. Mol. Struct. 1128 (2017) 653–664.
[30] C.A. Lipinski, F. Lombardo, B.W. Dominy, P.J. Feeney,Experimental and computational approaches to estimate solubility and permeability in drug discovery and development settings, Adv Drug Deliv Rev. 46 (1-3) (2001) 3–26.
[31] D.F. Veber, S.R. Johnson, H.Y. Cheng, B.R. Smith, K.W. Ward, K.D. Kopple, Molecular properties that influence the oral bioavailability of drug candidates, J. Med. Chem. 45 (12) (2002) 2615–2623.
[32] A.B. Nielsen, A.J. Holder, Gauss View 5.0, User's Reference, GAUSSIAN Inc., Pittsburgh, PA, 2008.
[33] M.J. Frisch, G.W. Trucks, H.B. Schlegel, G.E. Scuseria, M.A. Robb, J.R. Cheeseman, G. Scalmani, V. Barone, B. Mennucci, G.A. Petersson, H. Nakatsuji, M. Caricato, X. Li, H.P. Hratchian, A.F. Izmaylov, J. Bloino, G. Zheng, J.L. Sonnenberg, M. Hada, M. Ehara, K. Toyota, R. Fukuda, J. Hasegawa, M. Ishida, T. Nakajima, Y. Honda, O. Kitao, H. Nakai, T. Vreven, J.A. Montgomery Jr., J.E. Peralta, F. Ogliaro, M. Bearpark, J.J. Heyd, E. Brothers, K.N. Kudin, V.N. Staroverov, R. Kobayashi, J. Normand, K. Raghavachari, A. Rendell, J.C. Burant, S.S. Iyengar, J. Tomasi, M. Cossi, N. Rega, J.M. Millam, M. Klene, J.E. Knox, J.B. Cross, V. Bakken, C. Adamo, J. Jaramillo, R. Gomperts, R.E. Stratmann, O. Yazyev, A.J. Austin, R. Cammi, C. Pomelli, J.W. Ochterski, R.L. Martin, K. Morokuma, V.G. Zakrzewski, G.A. Voth, P. Salvador, J.J. Dannenberg, S. Dapprich, A.D. Daniels, O. Farkas, J.B. Foresman, J.V. Ortiz, J. Cioslowski, D.J. Fox, Gaussian 09, Revision A.02, Gaussian, Inc, Wallingford CT, 2009.
[34] E.D. Glendening, J.K. Badenhoop, A.D. Reed, J.E. Carpenter, F. Weinhold, NBO 3.1; Theoretical Chemistry Institute, University of Wisconsin; Madison, WI, 1996.
[35] B.H. Besler, K.M. Merz Jr., P.A. Kollman, Atomic charges derived from demi-empirical methods, J. Comput. Chem. 11 (1990) 431–439.
[36] F. Biegler-Köning, J. Schönbohm, D. Bayles, AIM2000; A program to analyze and visualize atoms in molecules, J. Comput. Chem. 22 (2001) 545.
[37] T. Sundius, Scaling of ab initio force fields by MOLVIB, Vib. Spectrosc. 29 (2002) 89–95.
[38] S.F. Boys, F. Bernardi, The calculation of small molecular interactions by the differences of separate total energies. Some procedures with reduced errors, Mol. Phys. 19 (1973) 553–566.
[39] R. Ditchfield, Self-consistent perturbation theory of diamagnetism. I. A gage-invariant LCAO (linear combination of atomic orbitals) method for NMR chemical shifts, Mol. Phys. 27 (1974) 714–722.
[40] P. Ugliengo, MOLDRAW Program, University of Torino, Dipartimento Chimica IFM, Torino, Italy, 1998.
[41] A.V. Marenich, C.J. Cramer, D.G. Truhlar, Universal solvation model based on solute electron density and a continuum model of the solvent defined by the bulk dielectric constant and atomic surface tensions, J. Phys. Chem. B 113 (2009) 6378–6396.
[42] J. Tomasi, J. Persico, Molecular interactions in solution: an overview of methods based on continuous distributions of the solvent, Chem. Rev. 94 (1994) 2027–2094.
[43] S. Miertus, E. Scrocco, J. Tomasi, Electrostatic interaction of a solute with a continuum, Chem. Phys. 55 (1981) 117–129.
[44] I. Caracelli, J. Iulek, A. Neves, I. Vencato, F. Silva Jnr, T.J. Brocksom, J. Zukerman-Schpector, Intermediates in the synthesis of cembrane diterpenes, Acta Cryst. C53 (1997) 1282–1284.
[45] I. Rodríguez-Escudero, J. Marrero, A.D. Rodríguez, Kallolide A acetate pyrazoline, Acta Cryst. E68 (2012) o41–o42.
[46] R.F.W. Bader, Atoms in Molecules. A Quantum Theory, Oxford University Press, Oxford, 1990. ISBN: 0198558651.
[47] R.G. Parr, R.G. Pearson, Absolute hardness: companion parameter to absolute electronegativity, J. Am. Chem. Soc. 105 (1983) 7512–7516.
[48] G. Keresztury, S. Holly, G. Besenyei, J. Varga, A.Y. Wang, J.R. Durig, Vibrational spectra of monothiocarbamates-II. IR and Raman spectra, vibrational assignment, conformational analysis and *ab initio* calculations of *S*-methyl-*N*,*N*-dimethylthiocarbamate, Spectrochim. Acta 49A (1993) 2007–2026.
[49] D. Michalska, R. Wysokinski, The prediction of Raman spectra of platinum(II) anticancer drugs by density functional theory, Chem. Phys. Lett. 403 (2005) 211–217.
[50] M.B. Márquez, S.A. Brandán, A Structural and vibrational investigation on the antiviral deoxyribonucleoside thymidine agent in gas and aqueous solution phases, Int. J. Quant. Chem. 114 (2014) 209–221.
[51] N. Issaoui, H. Ghalla, S.A. Brandán, F. Bardak, H.T. Flakus, A. Atac, B. Oujia, Experimental FTIR and FT-Raman and theoretical studies on the molecular structures of monomer and dimer of 3-thiopheneacrylic acid, J. Mol. Struct. 1135 (2017) 209–221.
[52] Available from UV-Vis phenol. http://webbook.nist.gov/cgi/cbook.cgi?ID=C108952&Mask=480#UV-Vis-Spec.
[53] T.J. Bruno, P.D.N. Svoronos, CRC Handbook of Basic Tables for Chemical Analysis, second ed., CRC Press, Taylor & Francis Goup, Boca Raton, 2011.
[54] R.A. Friedel, M. Orchin, Ultraviolet Spectra of Aromatic Compounds, Wiley & Sons, New York and London, 1951.